# Superionic Conductivity in Lithium-Rich Anti-Perovskites

Yusheng Zhao*,[†,‡] and Luke L. Daemen[‡]

[†]Department of Physics and Astronomy, University of Nevada, Las Vegas, Nevada 89154, United States

[‡]Los Alamos Neutron Science Center, Los Alamos National Laboratory, Los Alamos, New Mexico 87545, United States

**ABSTRACT:** Lithium ion batteries have shown great promise in electrical energy storage with enhanced energy density, power capacity, charge−discharge rates, and cycling lifetimes. However common fluid electrolytes consisting of lithium salts dissolved in solvents are toxic, corrosive, or flammable. Solid electrolytes with superionic conductivity can avoid those shortcomings and work with a metallic lithium anode, thereby allowing much higher energy densities. Here we present a novel class of solid electrolytes with three-dimensional conducting pathways based on lithium-rich anti-perovskites (LiRAP) with ionic conductivity of $\sigma > 10^{-3}$ S/cm at room temperature and activation energy of 0.2−0.3 eV. As temperature approaches the melting point, the ionic conductivity of the anti-perovskites increases to advanced superionic conductivity of $\sigma > 10^{-2}$ S/cm and beyond. The new crystalline materials can be readily manipulated via chemical, electronic, and structural means to boost ionic transport and serve as high-performance solid electrolytes for superionic $Li^+$ conduction in electrochemistry applications.
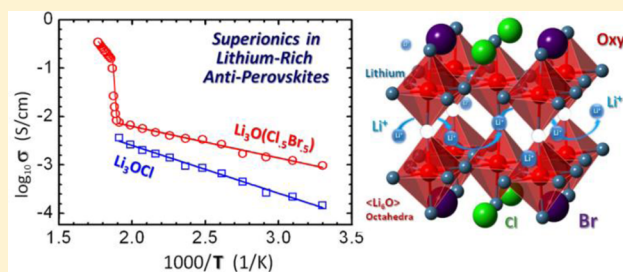
## INTRODUCTION

Lithium-based solid electrolytes[1] are attractive for battery applications as they have the potential to work well with metallic lithium anodes[2] at high voltage to provide enhanced performance in specific energy and power capacity.[3] To offer technological advantages in electrochemistry applications it must also meet a number of criteria besides high ionic conductivity: (a) low electronic conductivity with minimum self-discharge for long shelf life; (b) large working windows in voltage and current; (c) stable operation in a broad temperature range from −100 °C up to 300 °C; (d) low leakage, low electrode corrosion, and good thermomechanical strength to allow for easy packaging with the ability to survive abusive environments; and (e) low cost, lightweight, and low toxicity, i.e. economical and environmental friendliness.
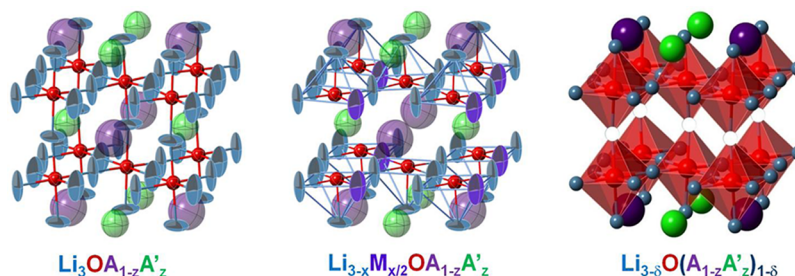
Inspired by the high temperature superionic conductivity of $NaMgF_3$ and $(K,Na)MgF_3$ perovskites,[4−7] we propose a novel family of "electronically-inverted" anti-perovskites, e.g., $ClOLi_3$ and $(Cl,Br)OLi_3$, as Li-rich superionic conductors. In the typical $A^+B^{2+}X^-_3$ perovskite structure, A ($Na^+$) is a monovalent metallic cation, B ($Mg^{2+}$) is a divalent metallic cation, and X ($F^-$) is a strongly electronegative monovalent anion. To obtain a $Li^+$ ionic conductor, we replace the electronegative anion element in the traditional perovskite system (e.g., fluorine in $NaMgF_3$) by the electropositive lithium metal, and continue the electronic inversion to $A^-B^{2-}X^+_3$, where $A^-$ is now a monovalent anion, $B^{2-}$ is a divalent anion, and $X^+$ is a strongly electropositive monovalent cation, namely $Li^+$, located at the octahedral vertices. The divalent anion element at the octahedral center (B-site) is conveniently chosen as oxygen, and the monovalent anion element at the dodecahedral center (A-site) can be any halogen (F, Cl, Br, I) or a mixture of halogens. The perovskite structure is preserved in the newly designed compound $ClOLi_3$, which should allow $Li^+$ superionic conduction by analogy with $F^-$ superionic conductivity in $NaMgF_3$. The resulting "electronically-inverted" anti-perovskite crystalline solid is lithium-rich (29 wt % or 60 at % Li in $ClOLi_3$) and lightweight. Following the "cation-first" convention in the usual inorganic nomenclature of ionic compounds, we henceforth reverse the suggestive notation $A^-B^{2-}X^+_3$ to the anti-perovskite notation defined as: $X^+_3B^{2-}A^-$; thus, the lithium-rich anti-perovskite (LiRAP) will now be denoted $Li_3OCl$, rather than $ClOLi_3$.

We noted later on that Schwering et al. had studied a similar anti-perovskite system based on the composition $Li_{3-n}(OH_n)X$ (X = Cl, Br; 0.83 < n < 2).[8] Rather interestingly, in the study by Schwering et al. the structural phase transition to the cubic phase was accompanied by a significant jump in the Li ionic conductivity of $Li_2(OH)Cl$ by 3 orders of magnitude to reach $10^{-4}$ S·cm$^{-1}$ above room temperature. Unlike the compounds studied by Schwering et al., the family of compounds proposed in the present study has a different generic composition. Our compounds will not dehydrate upon heating and remain usable as electrolytes even in the molten state. Decomposition of $Li_3OCl$ does not occur until nearly 400 °C. The anti-perovskite structure is, of course, not new and includes numerous compounds incorporating Li and Mg (*see ref 8 for additional references on anti-perovskites*). However, it has received decidedly less attention than the perovskite class as a whole. Both families of compounds (*Schwering et al. and this article*) are undoubtedly of great interest to understand the nature of lithium ion transport in Li-rich electrolytes, in particular with respect to the effects of structural variations.

© 2012 American Chemical Society

15042

dx.doi.org/10.1021/ja305709z | *J. Am. Chem. Soc.* 2012, 134, 15042−15047

**Figure 1.** Anti-perovskite structure drawings to illustrate the effects of mixing (left), doping (mid), and depletion (right). The large thermal ellipsoids demonstrate the soft phonon effects and are drawn at 68% probability level.

## ■ EXPERIMENTAL SECTION

We have developed an efficient synthesis to produce a wide variety of Li-rich anti-perovskites. The first step of the synthesis of $Li_3OCl$ consists of grinding together 2 equiv of LiOH and 1 equiv of LiCl. In a typical synthesis, 2.40 g of LiOH (0.1 mol; Aldrich, > 99% purity) and 2.12 g of LiCl (0.05 mol; Aldrich, >99% purity) are ground together for several minutes with a mortar and pestle. The resulting paste is placed in a quartz tube and heated to 330−360 °C (past the melting point $T_m$ = 282 °C of the product) under vacuum for several days. During heating, water is effectively removed with a condensation (liquid nitrogen) trap and a high-vacuum pump. At the end of the reaction, the molten product in the quartz tube is rapidly quenched or slowly cooled to room temperature, which results in different textures and grain boundary morphologies. At the end of the synthesis, the apparatus is flushed with a dry inert gas (e.g., Ar) and the very hygroscopic sample is never subsequently exposed to atmospheric moisture. Continuous heating (*330−360 °C at melt*) and removal of water under high vacuum drive the chemical equilibrium toward the formation of the $Li_3OCl$ product:

$$LiCl + 2LiOH \rightarrow Li_3OCl + H_2O \qquad (1)$$
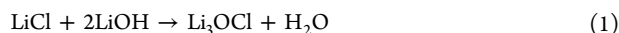
The reaction in the molten state is simple, and the sample is obtained as a white, dense, hard polycrystalline mass. We have also performed high-*P*/high-*T* synthesis from $Li_2O$ and LiCl and obtained the same polycrystalline anti-perovskite samples through a different reaction path. Pressing on the reagent mixture helps push the diffusion-limited solid state reaction to completion by maintaining good contact between the reagents. The high-*P*/-*T* synthesis is favored thermodynamically for such solid state reactions as well; however, only small amounts of the sample could be recovered by this method, and we did not pursue this synthesis method further.

To the best of our knowledge, the $Li_3OCl$ anti-perovskite is reported here for the first time and our molten synthesis approach is entirely novel and can be scaled up easily to produce large quantities of product.

Anti-perovskites can be structurally manipulated quite easily by chemical substitution, e.g. by introducing large $Br^-$ anions at the dodecahedral site to replace $Cl^-$ anions. The use of mixed halogens (e.g., $Cl_{1−z}Br_z$) can push the tolerance factor: $t = (r_A + r_X)/[\sqrt{2}\,(r_B + r_X)]$ of the anti-perovskite to vary from 0.85 for pure $Li_3OCl$ to 0.91 for pure $Li_3OBr$ as the substitution goes from the chlorine end-member to the bromine end-member. A higher tolerance factor indicates that the anti-perovskite structure approaches a less distorted pseudocubic phase. This, in turn, promotes the displacive structural phase transition controlled by phonon softening. The eutectic effect also reduces the melting and phase transition temperatures in the anti-perovskite with mixed halogens. Such structural manipulations should promote superionic conduction via *Frenkel* interstitial transport.

In general, mixed-halogen compositions of Li-rich anti-perovskites can be obtained easily with simple modifications of the synthesis described above, e.g. $Li_3OA_{1−z}A'_z$ where A and A' are distinct A-site halogens (F, Cl, Br, I) can be prepared as, Figure 1 (left):

$$2LiOH + (1 − z)LiA + zLiA' \rightarrow Li_3OA_{1−z}A'_z + H_2O \qquad (2)$$
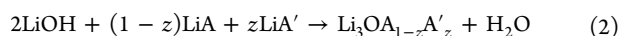
Similarly, cationic doping is easily achieved, as shown in reaction 3:

$$2LiOH + (x/2)MA_2 + (1 − x)LiA \rightarrow Li_{3−x}M_{x/2}OA + H_2O \qquad (3)$$
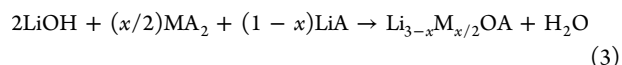
where A is a halogen at the dodecahedral site and M is a divalent metal (*e.g.*, an alkaline earth element such as $Mg^{2+}$) replacement at the $\langle Li_6O \rangle$ octahedral center. (*The* reaction *is trivially modified for higher-valent metals.*) This will produce a material with increased concentration of electronic vacancies at the Li sites in the anti-perovskite lattice—so as to promote neighboring ionic hopping via the *Schottky* route—a well-known doping method to increase ionic conductivity in ionic solids.[9] The idea is to configure an anti-perovskite structure with fast ionic channels in which the vacant Li sites line up in a more or less ordered fashion, Figure 1 (middle).

Naturally, it is possible to combine the synthesis reactions 2 and 3 to produce materials with more general anti-perovskite compositions: $Li_{3−x}M_{x/2}OA_{1−z}A'_z$. The charge and size of M, A, and A' permit the manipulation of the anti-perovskite crystal lattice and electronic structure. The resulting "vacancy-enhanced" and "distortion-controlled" solid electrolyte materials represent a vast family of Li-rich anti-perovskites with excellent and easily manipulated $Li^+$ ionic conductivity.

We can also purposely deplete LiA to effectively introduce empty dodecahedral A-sites and Li vacancies at the octahedral vertex, Figure 1 (right), so as to control the structural distortion and produce lattice defects/channels for enhanced ionic conduction in the anti-perovskites. The depleted samples of $Li_{2.95}OCl_{0.95}$, $Li_{2.90}OCl_{0.90}$, $Li_{2.85}OCl_{0.85}$, and $Li_{2.80}OCl_{0.80}$, i.e. [ $Li_3OCl − (0.05, 0.10, 0.15, 0.20) \times (LiCl)$ ], were synthesized to generate the 5%, 10%, 15%, and 20% Cl depletion (empty A-sites) in the anti-perovskite with concurrent creation of 1.66%, 3.33%, 5%, and 6.66% Li vacancies (0.05/3, 0.10/3, 0.15/3, 0.20/3) due to the electronic balance rule. The molten synthesis of the "depleted" anti-perovskites is similar to above listed reactions:

$$(1 − \delta)LiA + 2LiOH \rightarrow Li_{3−\delta}OA_{1−\delta} + H_2O \qquad (4)$$
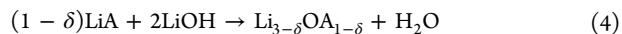
By integrating reactions 2, 3, and 4, even more general anti-perovskite compositions can be readily derived as $Li_{3−x−\delta}M_{x/2}O(A_{1−z}A'_z)_{1−\delta}$, which combines the effects of A-mixing, M-doping, and LiA-depletion to further control structural distortion and enhance $Li^+$ hopping for optimized lithium transport. The extent of mixing, doping, and depleting can be substantial as long as the anti-perovskite structures remain stable! We may consider the Li-rich anti-perovskites as a "lithium swamp" that needs "trenches" to channel fast ionic transport. The combined manipulation via chemical, electronic, and structural means forms such three-dimensional (3D) "channels" to allow for easy $Li^+$ hopping and transport.

We speculate that the soft phonon-driven structural phase transitions in the anti-perovskites can actively promote lithium transport. The associated large thermal ellipsoid suggests high $Li^+$ mobility, as shown in the ORTEP drawing, Figure 1 (left and middle). The lithium thermal motion in the anti-perovskite structure occurs within a flattened thermal ellipsoid path, i.e. in a shallow and flat energy well,[5,6] as happens in the "sub-lattice melting" state in the classic $\alpha$-AgI case,[10] near the structural phase transition. Such high mobility of the lithium cations in the octahedral structure allows

superionic conduction in the anti-perovskite lattice at high temperatures.

X-ray diffraction (XRD, Rigaku Ultima III instrument) reveals that $Li_3OCl$ and $Li_3OBr$ have the typical perovskite crystal structure, Figure 2, albeit with minor distortions from the ideal cubic structure (#221,
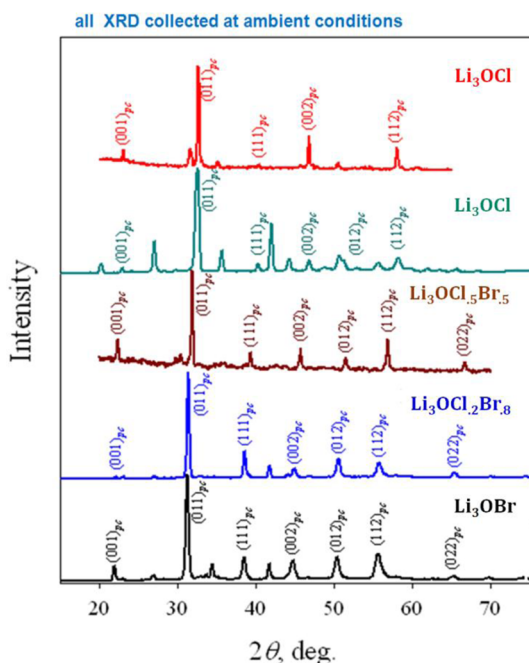


**Figure 2.** X-ray diffraction patterns of $Li_3OCl$, $Li_3OBr$, and mixed $Li_3O(Cl,Br)$ anti-perovskites collected at room temperature. The major diffraction peaks are indexed with Miller indices for the pseudocubic perovskite structure. The two diffraction patterns with limited $2\theta$ range are data collected with samples made via the high-temperature melting process. The other diffraction patterns are data collected with the samples synthesized via the high-pressure/-temperature route.

$Pm3m$) typical of perovskites.[11] The XRD patterns in Figure 2 are indexed with Miller indices corresponding to the pseudocubic structure. The lattice parameters are 3.91 Å and 4.02 Å for $Li_3OCl$ and $Li_3OBr$, respectively, with one formula unit per unit cell ($Z = 1$) for a typical cubic structure. The mixed phases of the $Li_3O(Cl_{1-z}Br_z)$ anti-perovskite show a good solid—solution of two end members. Most samples, especially near room temperature, exhibit small extra Bragg

peaks in their X-ray diffraction pattern. These are due to small tetragonal or orthorhombic distortions from the ideal cubic structure. These distortions are typical of many perovskites. The observed distortion is somewhat dependent on the rate of sample cooling at the end of the synthesis. At high temperature, many of these small extra Bragg peaks disappear as the structure (statically or dynamically) is closer on average to the ideal cubic structure. The crystallography of perovskites at the level of local disorder can be extremely complex and is beyond the scope of this article. It should also be noted that the samples tend to be textured, as reflected in varying relative Bragg peak intensities for samples with identical compositions. Texture depends on cooling rates at the end of the synthesis.

Structural changes, including melting, in anti-perovskites were observed with a simple thermal analysis approach. We performed differential scanning calorimetry (DSC, Netzsch, Jupiter 449C) measurements on the anti-perovskite samples. The results are shown in Figure 3. The last peak at high temperature (heating) is the melting phase transition. The mixed-halogen compound has a lower melting point than the two parent end members. There is a small endothermic peak in the $Li_3OCl$ sample around 40 °C and another even smaller one at around 225 °C during heating. In some perovskites, this is due to a change in local order, e.g. octahedral tilting along one particular lattice axial direction. It corresponds to the unfolding of either the $M_3$ point and/or the $R_{25}$ point of the Brillouin zone in lattice dynamics. XRD does not reveal anything remarkable at temperatures below or above these peaks other than slight changes in the intensity of the superlattice peaks, which confirms that the appearance of small, extra Bragg peaks in the diffraction pattern is related to modest structural changes resulting in tetragonal or orthorhombic distortion of the structure. Melting occurs at 282 °C for the $Li_3OCl$ sample, but the onset of melting occurs some 10 degrees lower, Figure 3 (left). The $Li_3OBr$ sample displays the same weak endothermic feature as $Li_3OCl$, but at 206 °C. A new endothermic peak appears at 232 °C, below $T_m = 280$ °C, which represents the soft phonon-driven structural phase transition in the anti-perovskite.

The mixed halogens sample $Li_3OCl_{0.5}Br_{0.5}$ inherits this new feature of $Li_3OBr$ with a peak at 247 °C and with a lower melting point of 270 °C, Figure 3 (right). The DSC measurements of the sample $Li_3OCl_{0.5}Br_{0.5}$ during sample cooling shows three exothermic peaks, which correspond to nucleation of crystallites, ordering of the mixed halogens, and crystallization to the solid state. There are only two exothermic peaks (nucleation and crystallization) for the end member samples. As the halogens possess widely different ionic sizes, the substitution of halogens in the Li-rich anti-perovskites should be a very efficient method of structural manipulation.
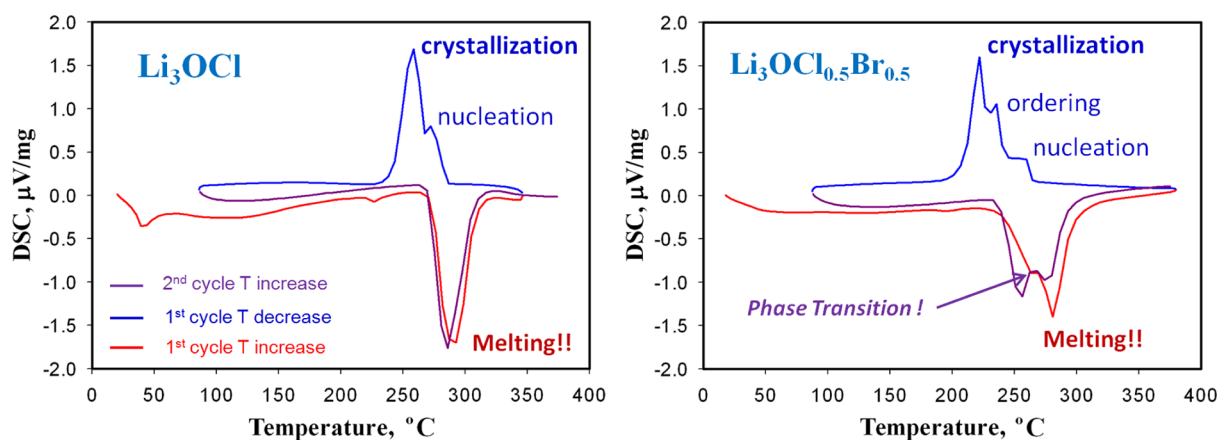


**Figure 3.** Differential Scanning Calorimetry (DSC) data collected at a heating rate of 5 °C min$^{-1}$ in a flow of dry argon gas. The observed thermodynamic events (phase transition, melting, nucleation, ordering, crystallization) are marked next to the DSC curve.

# RESULTS

Three typical impedance measurements at high temperatures are presented in Nyquist plots, Figure 4, of the real and
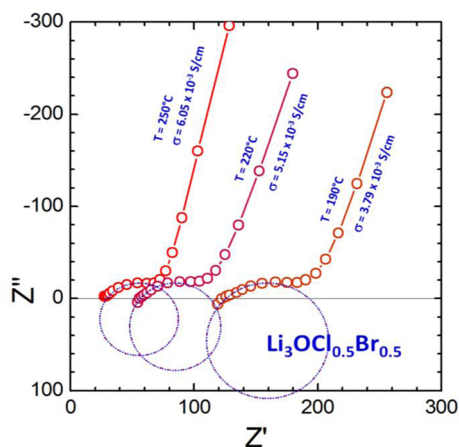


**Figure 4.** Impedance spectroscopy Nyquist plots of the real and imaginary components of the anti-perovskite impedance measured at different temperatures. The impedances are in ohms.

imaginary components of the impedance $Z$ for the electro-chemical circuit. An arc in the complex impedance plane demonstrates that the anti-perovskites behave as an electrolyte resistance in parallel with an inter-electrode capacitance. We also collected the relaxation spectra to show the frequency response of the electric resistances varying with temperature. The bulk ionic conductivity of the anti-perovskites can thus be quantified as a function of temperature, independent of electrochemical effects at electrodes.

Our measurements of ionic conductivity at room temperature derive the values of $0.85 \times 10^{-3}$ S/cm for the end member $Li_3OCl$ anti-perovskite and $1.94 \times 10^{-3}$ S/cm for the 50/50 mixed phase of $Li_3OCl_{0.5}Br_{0.5}$ anti-perovskite, respectively. These values boost to $4.82 \times 10^{-3}$ S/cm and $6.05 \times 10^{-3}$ S/cm as temperature increases to $T = 250$ °C.

The ionic conductivity measurements of the Li-rich anti-perovskites at high temperatures follow the typical Arrhenius plots, Figure 5, which reflects an increase of the ionic conductivity with temperature in an exponential fashion: $\sigma T = A_o \times \exp(-E_a/kT)$, where $E_a$ is the activation energy for ion
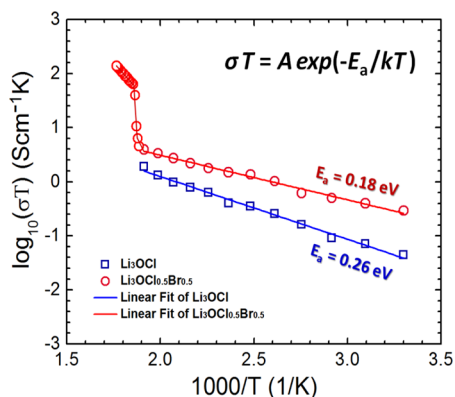


**Figure 5.** Arrhenius plots of $\log(\sigma T)$ versus $1/T$ for $Li_3OCl$ and $Li_3OCl_{.5}Br_{.5}$ anti-perovskites. The plot slopes are used to derive the activation energies $E_a$.

transport in the crystal lattice, $k$ is the Boltzmann constant, and $A_o$ is the intercept of the $\log(\sigma T)$ versus $1/T$ plot. The $E_a$ derived from the slopes of the Arrhenius plots are 0.26 and 0.18 eV for the $Li_3OCl$ and $Li_3OCl_{0.5}Br_{0.5}$ anti-perovskites, respectively, rather low values.

The $Li_3OCl$ and $Li_3OCl_{0.5}Br_{0.5}$ anti-perovskite data plotted in Figures 4 and 5 have the following specifications for sample preparation: (1) We kept the anti-perovskites in the molten state at a high temperature of 360 °C for a long period of time (approximately 100 h), to ensure complete water removal. During this process the volatile elements chlorine and/or bromine may have escaped from the crystal lattice in distinct amounts (*not in a controlled way, though; quantification of this process of Li and Cl removal is in progress*), and the corresponding amount of lithium may be reduced concurrently, as shown in Figure 1 (right), resulting in the "depleted" anti-perovskites noted as $Li_{3-\delta}OCl_{1-\delta}$ and/or $Li_{3-\delta}O(Cl_{0.5}Br_{0.5})_{1-\delta}$. (2) We poured and spread the molten anti-perovskite on a flat aluminum foil to form a "pancake" sample, we then cut the crystalline bulk into a disk-shaped sample without crushing it into a pellet so as to diminish grain boundary effects. Notice that the highly corrosive anti-perovskite melts may react with the aluminum foil and accidentally dope the anti-perovskites with $Al^{3+}$ cations (*again, not in a controlled way*), generating a high concentration of vacancies at the octahedral vertices due to the charge-balance rule (*this needs to be verified with a detailed chemical analysis*). (3) We used a sputtering technique to coat gold layers on the flat surfaces of the samples disks, as well as gold foils, to increase the sample contact at the electrode interfaces. We believe all of the above-mentioned precautions are important in the measurement of ionic conductivity of the $Li_3OCl$ and $Li_3O(Cl,Br)$ anti-perovskites.

The reason that the mixed-halogen phase $Li_3O(Cl,Br)$ shows a higher ionic conductivity than the end member anti-perovskites is likely due to its peculiar topological nature, Figure 1. The end member $Li_3OBr$ has large Br anions that almost completely fill the dodecahedral A-site of the anti-perovskite, which leaves little room for $Li^+$ cations to hop in the interstitial space. In the other end member, $Li_3OCl$, with smaller $Cl^-$ anions that are not large enough to fill the dodecahedral space substantially, the perovskite structure distorts via octahedral tilting, which results in (partially) collapsed A sites (the coordination goes from 12 to 8, correspondingly). This low-symmetry phase still leaves no significant channels for ionic transport. Alternating larger Br and smaller Cl anions in the dodecahedral A-sites in a 3D topology generates a larger unit cell closer to the end member $Li_3OBr$.[12] Simultaneously, it straightens the octahedral tilting, which results in a less distorted perovskite structure with larger 12-coordinated dodecahedra for the smaller Cl anion to reside. Such a topological setting provides free space in the chlorine-occupied dodecahedra for the $Li^+$ cations to hop in and pass through via the interstitial *Frenkel* route.

Advanced superionic conductivity is achieved eventually at high temperatures as significant structural disordering generates a large amount of vacancies for $Li^+$ on-site hopping, while the large thermal vibration of lithium at the vertices of the octahedral drastically enhances the ionic hopping probability. Whereas the two end member anti-perovskites, $Li_3OCl$ and $Li_3OBr$, reach superionic conducting of $\sigma > 10^{-2}$ S/cm at $T >$ 250 °C (about 30 degrees below the melting temperatures), as indicated by the significant jump at high temperatures (at $1/T < 1.9 \times 10^{-3}$ in Figure 5), the conductivity of the 50/50 mixed

halogens sample $Li_3OCl_{0.5}Br_{0.5}$ goes above $10^{-2}$ S/cm (1 S/m) at an even lower temperature of 232 °C, then quickly achieves advanced superionic conduction of $10^{-1}$ S/cm (10 S/m) at 248 °C, and eventually gets to $10^0$ S/cm (100 S/m) at 266 °C. The ionic conductivity of the anti-perovskites is comparable to that of other actively studied lithium conductors such as $Li_3N$ and $Li_7La_3Zr_2O_{12}$,[13−16] or $Li_{10}GeP_2S_{12}$.[17] It is also comparable to that of some liquid electrolytes.[18]

The ionic conductivity of the anti-perovskites can be further improved by introducing transport channels via doping and/or depleting, as illustrated in Figure 1, mainly to promote the lithium/vacancy on-site hopping and/or to pass through the free spaces of the empty dodecahedral A-sites. The deliberate and combined approaches of A-mixing, M-doping, and LiA-depleting can optimize anti-perovskites $Li_{3−x−\delta}M_{x/2}O$-$(A_{1−z}A'_z)_{1−\delta}$ to achieve much higher superionic conductivity.

## ■ DISCUSSION

The lithium-rich anti-perovskites are highly hygroscopic and should not be exposed to atmospheric moisture. We performed synthesis, material handling, and all subsequent measurements in dry glove boxes with controlled dry inert atmosphere. It is also important to indicate that the derived ionic conductivity data are dependent on the sample preparation and measurement processes. In early measurements, all three samples of $Li_3OCl$, $Li_3OBr$, and $Li_3OCl_{0.5}Br_{0.5}$ showed rather low ionic conductivities in the range of $10^{-7}$ S/cm at room temperature. Upon annealing in vacuum above 250 °C (but below the melting point) for 24 h, the measured ionic conductivity showed significant improvement, by as much as 2 orders of magnitude. This was also accompanied by a change in the slope of the Arrhenius curve, denoting a change in activation energy for Li transport. These changes are most likely indicative of structural changes (e.g., octahedral tilting), grain boundary changes, and migration of vacancies. As noted above, texture appears as a result of different cooling rates at the end of sample synthesis. The subsequent thermal/physical history of a sample (annealing, heating/cooling, pressing, thermal/electrochemical history, etc.) seems to affect the measured conductivity to a greater or lesser extent.

Although the material is lithium-rich, the $Li^+$ cations are bonded tightly at the octahedral vertices and coordinated with two oxygen anions as nearest neighbor, which provides no ionic hopping mechanism and thus results in low conductivity in our early low-temperature measurements. It may be mainly due to the lack of vacancies in the crystal structure, i.e. sluggish ionic hopping via the *Schottky* route for the neighboring lattice sites. The situation gradually changes as temperature increases, and structure disordering occurs in association with enhanced thermal vibration. This is particularly true for the lithium sites where the thermal vibration shows much larger magnitude at high temperatures when phonon softening occurs.

It is important to notice that thermal treatment history and pellet texture influence the conductivity results significantly. Crystallization kinetics, texture formation and evolution, octahedral tilting, and grain boundaries affect microstructure, and, therefore, ionic conductivity. Slow structural relaxation effects have been observed over a period of days. These effects are not new and can be particularly pronounced in some perovskites. Such materials science issues are currently under systematic study and the results will be reported in a separate publication. For consistency, pellets for ionic conductivity measurements have been prepared following standard techniques of pressing or melting under inert atmosphere, and followed by prolonged annealing (> 24 hours) in vacuum at temperatures varying between 150 °C and 250 °C. A sputter coater is then used to deposit gold contacts on each side of the pellet. Gold foils (100 microns) are placed between the sputtered gold contacts on the pellet and the brass/copper electrodes used in our measurements. Spring loading maintained good contact between the electrodes and the pellet.

The complete elucidation of the connection between local disorder, thermal history, and microstructure is in progress. This is a critical investigation to assess microstructural and electrochemical stability. Our best samples for conductivity measurements were obtained after long thermal annealing in vacuum-melted pellets subsequently coated with a thin film of gold. It is foreseeable that the ionic conductivity of the novel lithium-rich anti-perovskite superionic solid electrolytes still has great room to improve, not only through chemical/electronic/structural manipulations but also via sample preparation/handling and optimization of measurement processes.

## ■ CONCLUSION

The perovskite structure is ubiquitous in nature. Compounds with the perovskite structure display an amazing array of physical properties: ferroelectricity, superconductivity, exotic magnetism, etc. Our new family of lithium-rich solid electrolytes based on the anti-perovskite adds to this extraordinary plethora of materials and properties. While interesting for their crystal structure and superionic conductivity, the Li-rich anti-perovskites may also represent advances in electrochemistry systems as a cathode material with all sorts of possible cation and/or anion manipulations. Indeed, the low melting point of our anti-perovskites enables the straightforward fabrication of thin films—an important step toward the fabrication of layered compacts for high-performance battery/capacitor devices with existing technology. The anti-perovskites have the highest Li concentration of all Li-based solid electrolytes proposed so far; display superionic conductivity, low activation energy, and very low electronic conductivity; and offer potential for a large operation window in voltage and current. The products are lightweight and can be formed easily into sintered compacts. Our anti-perovskites are readily decomposed by water to lithium hydroxide and lithium halides of low toxicity and are therefore completely recyclable and environmentally friendly. The low cost of the starting materials and easy synthesis of the products in large quantities suggest economical advantages as well. The Li-rich anti-perovskites (LiRAP) have great potential for structural manipulation and electronic tailoring. We have only explored a very small portion of the vast field of research offered by this new class of materials. We expect future advances exploiting the ideas described above to attain even higher superionic conductivity and to develop solid electrolyte applications for various electrochemical devices.

## ■ AUTHOR INFORMATION

**Corresponding Author**
yusheng.zhao@unlv.edu
**Notes**
The authors declare no competing financial interest.

## ■ ACKNOWLEDGMENTS

## ■ REFERENCES

(1) Sunandana, C. S.; Kumar, P. S. *Bull. Mater. Sci.* **2004**, *27*, 1−17.

(2) Beattie, S. D.; Manolescu, D. M.; Blair, S. L. *J. Electrochem. Soc.* **2009**, *156* (1), A44−A47.

(3) Xu, K. *Chem. Rev.* **2004**, *104*, 4303−4417.

(4) O'keeffe, M.; Bovi, J.-O. *Science* **1979**, *206*, 599−600.

(5) Zhao, Y.; Weidner, D. J.; Parise, J. C.; Cox, D. *Phys. Earth Planet. Inter.* **1993**, *76*, 1−34.

(6) Zhao, Y. *J. Solid State Chem.* **1998**, *141*, 121−132.

(7) Yoshiasa, A.; Sakamoto, D.; Okudera, H.; Sugahara, M.; Ota, K.; Nakatsuka, A. *Z. Anorg. Allg. Chem.* **2005**, *631*, 502−506.

(8) Schwering, G.; Hönnerscheid, A.; van Wüllen, L.; Jansen, M. *ChemPhysChem* **2003**, *4*, 343−348.

(9) Chandra, S. *Superionic Solids: Principles and Applications*; Elsevier, North-Holland: North Holland, 1981.

(10) Cava, R. J.; Reidinger, F.; Wuensch, B. J. *Solid State Commun.* **1977**, *24*, 411.

(11) MegawH. D. *Crystal Structures: A Working Approach*; Saunders: Philadelphia, 1973.

(12) Wortmann, R.; Sitta, S.; Sabrowsky, H. *Z. Naturforsch., B: Chem. Sci.* **1989**, *44*, 1348−1350.

(13) Alpen, U. v.; Rabenau, A.; Talat, G. H. *Appl. Phys. Lett.* **1977**, *30*, 621−623.

(14) Li, W.; Wu, G.; Araújo, C. M.; Scheicher, R.h H.; Blomqvist, A.; Ahuja, R.; Xiong, Z.; Feng, Y.; Chen, P. *Energy Environ. Sci.* **2010**, *3*, 1524−1530.

(15) Murugan, R.; Thangadurai, V.; Weppner, W. *Angew. Chem., Int. Ed.* **2007**, *46*, 7778−7781.

(16) Kuhn, A.; Narayanan, S.; Spencer, L.; Goward, G.; Thangadurai, V.; Wilkening, M. *Phys. Rev. B* **2011**, *83*, 094302.

(17) Kamaya, N.; Homma, K.; Yamakawa, Y.; Hirayama, M.; Kanno, R.; Yonemura, M.; Kamiyama, T.; Kato, Y.; Hama, S.; Kawamoto, K. *Nat. Mater.* **2011**, *10*, 682−686.

(18) Wenige, R.; Niemann, M.; Heider, U.; Jungitz, M.; Hilarius, V. Liquid Electrolyte Systems for Advanced Lithium Batteries. http://www.cheric.org/PDF/Symposium/S-J2-0063.pdf; Chemical Engineering Research Information Center (KR), 1998; pp63−76.